electronic reprint

STRUCTURAL SCIENCE
CRYSTAL ENGINEERING
MATERIALS

ISSN: 2052-5206
journals.iucr.org/b

New insights on the $GeSe_xTe_{1-x}$ phase diagram from theory and experiment

Markus Guido Herrmann, Ralf Peter Stoffel, Michael Küpers, Mohammed Ait Haddouch, Andreas Eich, Konstantin Glazyrin, Andrzej Grzechnik, Richard Dronskowski and Karen Friese

Acta Cryst. (2019). B**75**, 246–256

Acta Cryst B
STRUCTURAL SCIENCE
CRYSTAL ENGINEERING
MATERIALS

ISSN 2052-5206

New insights on the $GeSe_xTe_{1-x}$ phase diagram from theory and experiment

Markus Guido Herrmann,[a] Ralf Peter Stoffel,[b] Michael Küpers,[b] Mohammed Ait Haddouch,[a] Andreas Eich,[c] Konstantin Glazyrin,[d] Andrzej Grzechnik,[c] Richard Dronskowski[b] and Karen Friese[a]*

[a]Jülich Centre for Neutron Science-2/Peter Grünberg Institute-4, Forschungszentrum Jülich GmbH, Wilhelm-Johnen Strasse, Jülich 52428, Germany, [b]Chair of Solid-State and Quantum Chemistry, Institute of Inorganic Chemistry, RWTH Aachen University, Landoltweg 1, Aachen 52056, Germany, [c]RWTH Aachen, Institute for Crystallography, Jägerstrasse 17-19, Aachen 52066, Germany, and [d]Photon Sciences, Deutsches Elektronen-Synchrotron, DESY, Notkestrasse 85, Hamburg 22607, Germany. *Correspondence e-mail: k.friese@fz-juelich.de

Received 28 November 2018
Accepted 31 January 2019

Edited by S. Parsons, University of Edinburgh, Scotland

Keywords: $GeSe_xTe_{1-x}$ solid solutions; temperature-dependent powder diffraction; first-principles calculations; high-pressure behaviour; bulk moduli.

CCDC reference: 1881565

Supporting information: this article has supporting information at journals.iucr.org/b

The high-pressure and low-temperature behaviour of the $GeSe_xTe_{1-x}$ system (x = 0, 0.2, 0.5, 0.75, 1) was studied using a combination of powder diffraction measurements and first-principles calculations. Compounds in the stability field of the GeTe structure type (x = 0, 0.2, 0.5) follow the high-pressure transition pathway: GeTe-I ($R3m$) → GeTe-II (f.c.c.) → GeTe-III ($Pnma$). The newly determined GeTe-III structure is isostructural to β-GeSe, a high-pressure and high-temperature polymorph of GeSe. Pressure-dependent formation enthalpies and stability regimes of the $GeSe_xTe_{1-x}$ polymorphs were studied by DFT calculations. Hexagonal Ge_4Se_3Te is stable up to at least 25 GPa. Significant differences in the high-pressure and low-temperature behaviour of the GeTe-type structures and the hexagonal phase are highlighted. The role of Ge···Ge interactions is elucidated using the crystal orbital Hamilton population method. Finally, a sketch of the high-pressure phase diagram of the system is provided.

1. Introduction

Binary chalcogenides of group IV–VI elements, *e.g.* GeTe, are narrow-gap semiconductors and potential candidates for numerous applications in optoelectronic (Okoye, 2002; Cardona & Greenaway, 1964) and thermoelectric (Levin *et al.*, 2013; Lee *et al.*, 2014; Li *et al.*, 2017) devices as well as for non-volatile phase-change memories (Shportko *et al.*, 2008; Lencer *et al.*, 2008). For GeTe, many substituents have been tested in order to improve its transport properties. It has been shown that incorporating Se (Yang *et al.*, 2016; Perumal *et al.*, 2016) influences the thermoelectric properties of GeTe and leads to an increase in the figure of merit, ZT, of up to 26% in the temperature range 300–800 K.

Under ambient conditions, GeTe crystallizes in a rhombohedral structure (GeTe-I; space group $R3m$) which can be described as a distorted variant of a face-centred cubic lattice (f.c.c.) (Leger & Redon, 1990; Onodera *et al.*, 1997) (Fig. 1). The Ge atom is incorporated in Peierls-distorted octahedra and shows a [3 + 3] coordination formed by three long and three short Ge—Te bonds (Leger & Redon, 1990; Onodera *et al.*, 1997). Alternatively, the structure can be described as being composed of layers of six-membered Ge—Te rings arranged in the chair-conformation which are stacked along the [001] direction.

Mixed crystals in the $GeSe_xTe_{1-x}$ solid solution with $0 < x < 0.52$ are isostructural to GeTe-I (Wiedemeier & Siemers,

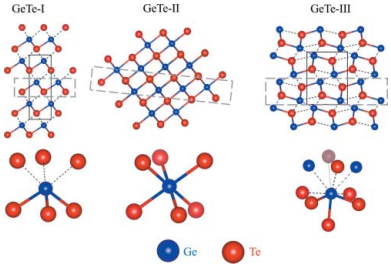

1984), while a hexagonal phase was observed for compounds with $0.58 < x < 0.85$ (Wiedemeier & Siemers, 1984). Recently, the crystal structure of $GeSe_{0.75}Te_{0.25}$ (in the following Ge_4Se_3Te) was determined in space group $P6_3mc$ (Küpers *et al.*, 2017; Fig. 1). The structure can be derived from the GeTe-I type by a rotation of 180° of every second layer around the [010] direction. This leads to a reduction in the number of Ge—Te bonds and the formation of additional Ge—Ge bonding interactions (Küpers *et al.*, 2017), resulting in the octahedral coordination of Ge with three Ge—Te and three Ge—Ge bonds.

Selenium-rich mixed crystals with $x > 0.95$ are isostructural to GeSe-I [space group *Pbnm* (Wiedemeier & Siemers, 1984; Wiedemeier & von Schnering, 1978), see Fig. 1]. As in GeTe-I, the structure is formed by layers of six-membered rings, yet the Ge—Se rings show a significantly different arrangement from the Ge—Te rings (Fig. 1; Wiedemeier & von Schnering, 1978).

At high temperatures, all phases in the $GeSe_xTe_{1-x}$ system undergo a phase transition to an f.c.c. structure isostructural to GeTe-II (Wiedemeier & Siemers, 1984). Only limited information on their low-temperature behaviour is available. The occurrence of two new Raman modes in GeSe below 150 K was attributed to a possible phase transition (Fukunaga *et al.*, 1981), but no structural information on the low-temperature phase was provided. Other authors report that GeSe-I is stable down to at least 70 K (Taube *et al.*, 2016). The lattice dynamics of rhombohedral GeTe at 30 K was studied using nuclear inelastic scattering (Bauer Pereira *et al.*, 2013) and the heat capacity data of this phase was determined between 1.2 and 22 K (Lewis, 1974). Finally, below 0.05 K, a superconducting phase was reported based on susceptibility measurements (Hein *et al.*, 1964).

GeTe-I undergoes a phase transition to GeTe-II at high pressure. However, the order of this phase transition remains unclear and the transition pressure p_{tr} depends strongly on the degree of hydrostaticity (Leger & Redon, 1990; Onodera *et al.*, 1997; Serebryanaya *et al.*, 1995), ranging from 3 GPa (Onodera *et al.*, 1997) to 8 GPa (Leger & Redon, 1990) for the hydrostatic and 3.5 (Serebryanaya *et al.*, 1995) to 5 GPa (Leger & Redon, 1990) for the non-hydrostatic conditions. Under non-hydrostatic conditions, the transition is accompanied by a volume reduction of about 3–3.5% (Leger & Redon, 1990; Serebryanaya *et al.*, 1995). At about 18–19 GPa, GeTe-II presumably transforms into an orthorhombic GeTe-III phase (Onodera *et al.*, 1997; Karbanov *et al.*, 1968), yet there are discrepancies with respect to the lattice parameters and the symmetry of this phase. Karbanov *et al.* (1968) proposed the space group *Pnma* and assumed the structure to be isostructural to GeSe-I. On the other hand, Onodera *et al.* (1997) suggested *Pbcn* symmetry and the presence of Ge—Te chains instead of six-membered rings. However, in neither of the two publications was a full structural refinement carried out and – in addition – unreasonably short Ge—Te distances are present in the structural model suggested by Onodera *et al.* (1997). At about 38 GPa, GeTe-III undergoes a phase transition to the CsCl type structure of GeTe-IV (Serebryanaya *et al.*, 1995).

A phase transition from the GeSe-I to the GeSe-II structure (space group *Ccmm*) was reported for a thin film of GeSe below 40 GPa (Xu *et al.*, 2017), analogous to the transitions reported for isostructural SnS (Alptekin & Durandurdu, 2010) and SnSe (Zhang, 2015). In contrast to this, a polycrystalline sample of GeSe did not show any phase transition below 82 GPa (Onodera *et al.*, 1997). Moreover, a new GeSe polymorph, so-called β-GeSe, was synthesized at high pressure and temperature. β-GeSe is quenchable to ambient conditions and crystallizes in the orthorhombic space group *Pnma* (Fig. 1) (von Rohr *et al.*, 2017). The structure consists of layers of six-membered Ge—Se rings arranged in the *boat* conformation.

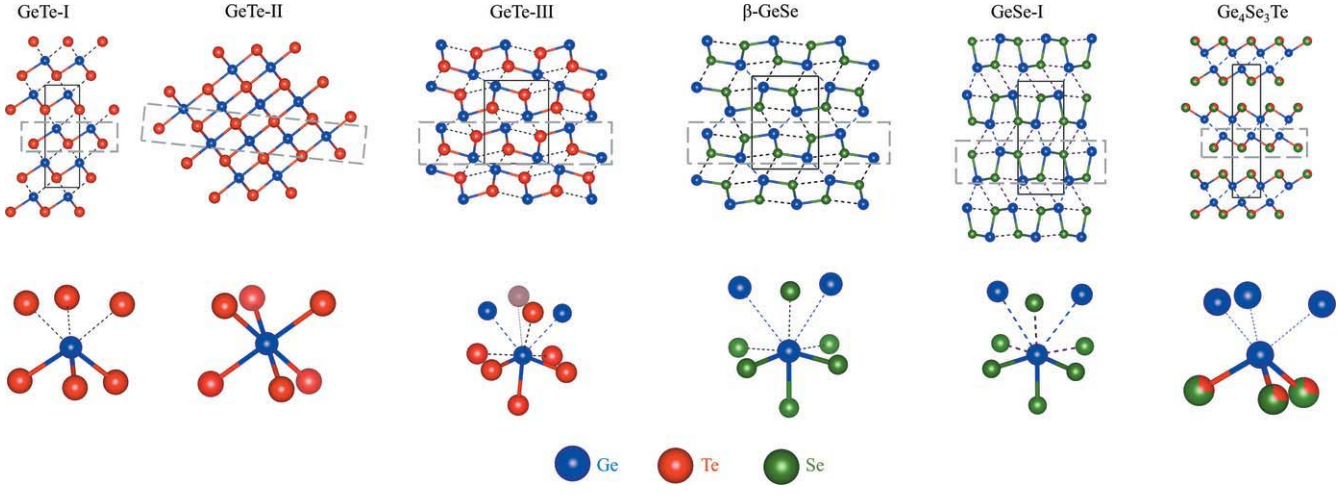

Figure 1
Comparison between the different phases of the $GeSe_xTe_{1-x}$ solid solution and corresponding coordination polyhedral around Ge: GeTe-I (Leger & Redon, 1990; Onodera *et al.*, 1997) and Ge_4Se_3Te (Küpers *et al.*, 2017), projections on the *bc* plane; GeTe-III and β-GeSe (Zhang *et al.*, 2015), projections on the *ac* plane; GeSe-I (Wiedemeier & von Schnering, 1978), projection on the *ab* plane; GeTe-II phase (Wiedemeier & Siemers, 1984), projections along the [110] direction.

The Ge atoms have a [3 + 3 + 2] coordination formed by six Ge—Se (three short, three long) and two Ge—Ge bonds (Zhang *et al.*, 2015).

As the low-temperature/high-pressure behaviour of the $GeSe_xTe_{1-x}$ mixed crystals is completely unknown and due to the aforementioned contradictions concerning the behaviour of the end members, we performed X-ray diffraction studies and DFT calculations on the crystals with x = 0, 0.2, 0.5, 0.75. We were particularly interested in elucidating how the Ge···Ge interactions affect the stability of the materials.

2. Experimental

2.1. Synthesis

Polycrystalline samples of $GeSe_xTe_{1-x}$ were synthesized from the elements Ge (MaTeck, 99.999%), Se (MaTeck, 99.999%) and Te (Alfa Aesar, 99.999%) in stoichiometric ratios. For each composition with x = 0, 0.2, 0.75, 1, a total mass of 200 mg was vacuum-sealed in quartz ampoules, heated to 900°C within 1–2 h, held at this temperature for 10 h, cooled to 300°C over 30 h and kept at this temperature for 24 h, followed by quenching in air. For the polycrystalline sample of $GeSe_{0.5}Te_{0.5}$, the elements were alloyed in a Fritsch 'Pulverisette 7 premium' planetary ball mill (in total: 3 g sample mass; milling time: 40 h with 5 min cycles and 3 min pauses at 600 rpm under an argon atmosphere; grinding bowl: 20 ml, ZrO_2 grinding balls: 10 × 1 cm). Afterwards, the sample was pressed to a 150 mg pellet and heated to 500°C in a glass ampoule under an argon atmosphere for 1 h, kept at 500°C for 1 h, followed by cooling to room temperature over 20 h. The phase purity of all samples was confirmed by X-ray powder diffraction.

2.2. Low-temperature powder diffraction

Low-temperature powder diffraction data were collected using a Huber G670 Guinier Camera equipped with a closed-cycle He cryostat and an image plate detector (Cu $K\alpha_1$; 2θ = 0–100°; $\Delta\theta$ = 0.005°). The samples were cooled to 25 K at a rate of 5 K min^{-1}. Data were collected every 5 K in the temperature range 25–300 K. Between the individual temperature points, the sample was heated up at a rate of 5 K min^{-1}, and a dwell time of 5 min was set in order to equilibrate the temperature.

2.3. High-pressure powder diffraction

High-pressure powder diffraction measurements on $GeSe_xTe_{1-x}$ (x = 0, 0.2, 0.5, 0.75) were performed at the beamline P02.2 of PETRA III (λ = 0.2905 Å) using a Perkin-Elmer detector (type XRD1621). The powders were loaded with small ruby chips in membrane driven BX90 diamond anvil cells (Kantor *et al.*, 2012) (culet size = 300 µm). Rhenium gaskets, pre-indented to a thickness of 80 µm and with a hole of 150 µm drilled by electro-corrosion, were used. Neon served as a pressure-transmitting medium. The ruby luminescence method (Mao *et al.*, 1986) was used to determine the pressure directly before and after each measurement. The maximum pressures were 20–21 GPa for GeTe and $GeSe_{0.2}Te_{0.8}$ and 25 GPa for $GeSe_{0.5}Te_{0.5}$ and Ge_4Se_3Te. The images were integrated to yield one-dimensional powder diffraction diagrams using the program *Dioptas* (Prescher & Prakapenka, 2015).

Table 1
Experimental details.

Crystal data	
Chemical formula	GeTe
M_r (g mol^{-1})	200.2
Crystal system, space group	Orthorhombic, *Pnma*
Temperature (K)	293
a, b, c (Å)	7.3690 (18), 3.9249 (10), 5.698 (9)
V (Å^3)	164.8 (3)
Z	4
Radiation type	Synchrotron, λ = 0.2905 Å
μ (mm^{-1})	10.39
Data collection	
Diffractometer	Perkin-Elmer XRD1621
No. of measured, independent and observed [$I > 3\sigma(I)$] reflections	135, 86, 84
R_{int}	0.040
(sin $\theta/\lambda)_{max}$ (Å^{-1})	0.825
Refinement	
$R[F^2 > 2\sigma(F^2)]$, $wR(F^2)$, S	0.047, 0.054, 2.39
No. of reflections	86
No. of parameters	13
$\Delta\rho_{max}$, $\Delta\rho_{min}$ (e Å^{-3})	2.11, −1.60

Computer programs: *CrysAlis PRO* (Rigaku, 2015), *SIR2014* (Burla *et al.*, 2015), *JANA2006* (Petricek *et al.*, 2014).

2.4. Le Bail refinements and single-crystal structure determination

All powder patterns at ambient and high pressures were refined with the Le Bail method (Pecharsky & Zavalij, 2003) using the program *JANA2006* (Petricek *et al.*, 2014). The background, described by 100 points, was fitted automatically using a 20-parameter polynomial function, and the zero-shift was refined. For the high-pressure data, the peak profiles were fitted with a pure Lorentzian function, while a pseudo-Voigt function was used for the refinements of the low-temperature data. Starting values for the lattice parameter were taken from the literature [GeTe-I (Bauer & Pereira *et al.*, 2013); GeTe-II (Wiedemeier & Siemers, 1984); $GeSe_{0.75}Te_{0.25}$ (Küpers *et al.*, 2017); GeSe-I (Wiedemeier & von Schnering, 1978)]. For GeTe at pressures above 13 GPa, new peaks appeared which we initially assumed would correspond to the GeTe-III phase described earlier in the literature. Surprisingly, the indexing of the new reflections using the lattice parameter corresponding to the two different models proposed for the GeTe-III phase by Karbanov *et al.* (1968) and by Onodera *et al.* (1997), respectively, failed. Yet in the dataset collected on GeTe at 18.8 GPa, single-crystal reflections appeared together with the powder pattern of our sample. These reflections were indexed with an orthorhombic unit cell [a = 7.3690 (18), b = 3.9249 (10), c = 5.698 (9) Å] using the program *CrysAlis PRO* (Rigaku, 2015). Based on the analysis of systematic extinctions and the internal agreement factor, the space group *Pnma* was

Table 2
Atomic coordinates and isotropic displacement parameters of the GeTe-III polymorph at 18.8 GPa.

Atom	Wyckoff position	x	y	z	U_{iso} (Å^2)
Ge	4c	0.0703 (13)	0.25	0.8267 (4)	0.025 (8)
Te	4c	0.1716 (5)	0.25	0.37428 (19)	0.019 (3)

chosen and the structure of GeTe-III was solved using direct methods implemented in the program *SIR2014* (Burla *et al.*, 2015). The subsequent refinement (Tables 1 and 2) was performed with the program *JANA2006* (Petricek *et al.*, 2014). All atoms were refined isotropically.

A careful inspection of the data for GeTe collected at higher and lower pressures showed a strong overlay of the powder rings with the single-crystal reflections of the new polymorph. It was therefore impossible to integrate the single-crystal reflections at other pressures reliably. However, based on the integrated powder diffraction patterns it was possible to extract the lattice parameters of GeTe-III in the pressure range 13.9–20.6 GPa. In addition, the diffraction pattern of $GeSe_{0.2}Te_{0.8}$ and $GeSe_{0.5}Te_{0.5}$ in the stability region of the orthorhombic phase was refined using the GeTe-III phase as a starting model.

2.5. DFT calculations

Density-functional theoretical calculations were carried out based on the projector-augmented wave method (Blöchl, 1994) implemented in the Vienna *ab initio* simulation package (*VASP*) (Kresse & Furthmüller, 1996; Kresse & Joubert, 1999). Plane-wave basis sets with an energetic cut-off of 500 eV were used, achieving a total energy convergence of well below 0.1 meV. The exchange and correlation were described by the local density approximation (LDA) in the formulation of Ceperley & Alder (1980) as parameterized by Perdew & Zunger (1981). This functional was chosen because it leads to a reasonable stabilization of the high-pressure GeTe-III structure at ambient (= 0 GPa) pressure, which was helpful for the investigation of the electronic bonding. In addition, a recent benchmark study on antimony telluride, Sb_2Te_3, led to the conclusion that the LDA functional performs satisfactorily for telluride materials (Stoffel *et al.*, 2015) and furthermore, this functional allowed for the successful modelling of the properties of bismuth telluride, Bi_2Te_3 (Zurhelle *et al.*, 2016), and antimony selenide, Sb_2Se_3 (Deringer *et al.*, 2015). The Brillouin zone was sampled on a dense mesh of reciprocal space points following the scheme of Monkhorst & Pack (1976) with at least 1000 k-points × atoms. Electronic wavefunctions were optimized until the difference between two iterative steps was well below 10^{-8} eV per atom. Structural optimizations were carried out until the energetic difference was below 10^{-6} eV. The initial structures for the simulations were GeTe-I (Bauer Pereira *et al.*, 2013), GeSe-I (Wiedemeier & von Schnering, 1978), the hexagonal structure of Ge_4Se_3Te (Küpers *et al.*, 2017) and the GeTe-III structure determined within this study. For each structure type and composition, three simulation cells were set up with randomly occupied Se/Te sites containing at least 48 atoms (24 formula units). GeTe-I was modelled with a 2 × 2 × 2 super cell related to the hexagonal setup, for the orthorhombic structures GeSe-II and GeSe-III, 1 × 3 × 2 super cells were used, and the simulation cell of the hexagonal Ge_4Se_3Te structure was set up as a 2 × 2 × 1 super cell. Because of the random occupation of the chalcogenide sites with Se and Te, the symmetry of the simulation cells was $P1$. First, structural optimizations with variable volume, cell shape and atomic positions were carried out until the pressure was approximately 0 GPa. This was followed by optimizations with fixed unit-cell volumes scaling the lattice vectors from 80 to 104% of the initial structure in steps of 1 or 2%, respectively. The so-obtained energy-volume data were used to fit the Murnaghan equation-of-state (Menoni *et al.*, 1986), resulting in values for the bulk modulus B_0, its pressure derivative $B' = dB/dp$, the equilibrium molar volume V_0 and the minimum electronic energy E_0. Furthermore, the enthalpy as a function of pressure was derived via the relation $H(p) = E[V(p)] + pV(p)$.

The bonding analysis was carried out using the program *LOBSTER* (Dronskowski & Bloechl, 1993; Deringer *et al.*, 2011; Maintz *et al.*, 2013, 2016) after having reconstructed the plane-wave data from *VASP* into local atomic orbitals of the contracted Slater type. For the bonding analysis, the GeTe-III structure was optimized with a constraint pressure of 15 GPa.

3. Results and discussion

3.1. Temperature-dependent powder diffraction

All detected peaks in the X-ray powder data for the five $GeSe_xTe_{1-x}$ samples under ambient conditions can be indexed with the lattice parameters reported in the literature (Küpers *et al.*, 2017; Wiedemeier & von Schnering, 1978; Bauer Pereira *et al.*, 2013), and no impurities were observed (see the supporting information). No additional peaks appear in any of the low-temperature powder diffraction diagrams and, in addition, no significant changes of the intensity ratios of the reflections are observed. Therefore, there is no indication of a phase transition in the temperature range 25–300 K in any of the samples.

For the isostructural compounds GeTe, $GeSe_{0.2}Te_{0.8}$ and $GeSe_{0.5}Te_{0.5}$, the a lattice parameter shows a positive thermal expansion, while the opposite is true for the c lattice parameter between 25 and 300 K (Fig. 2). The temperature-dependent behaviour of the a lattice parameter is hardly influenced by the Se content. The c lattice parameters are more strongly affected by the varying Se content with relative changes ranging from less than −0.1% for GeTe up to about −0.25% for $GeSe_{0.5}Te_{0.5}$ between 25 and 300 K. A negative thermal expansion in one crystallographic direction is a rare finding and, to the best of our knowledge, the only chalcogenide showing a similar thermal behaviour is the orthorhombic SnSe (Bansal *et al.*, 2016). The a lattice parameter of Ge_4Se_3Te also shows a positive thermal expansion, yet temperature-induced relative changes are about 0.2%, which

is much smaller compared with what is observed for the rhombohedral compounds (0.4%). The *c* lattice parameter of Ge_4Se_3Te indicates positive thermal expansion with relative changes of up to about 0.4%. This behaviour is in contrast with those observed for the rhombohedral compounds (Fig. 2). In general, the unit-cell volumes of all the $GeSe_xTe_{1-x}$ compounds (x = 0, 0.2, 0.5, 0.75) show a positive thermal expansion (see supporting information).

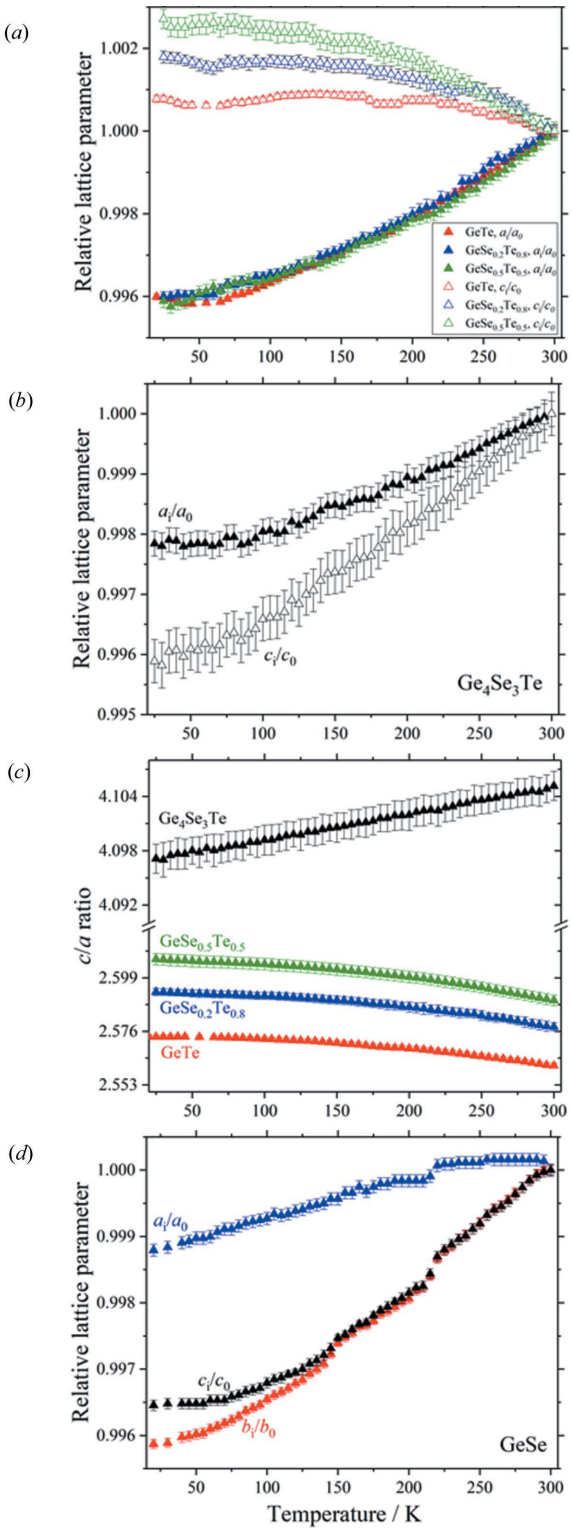

Figure 2
Temperature dependence of the normalized lattice parameters of rhombohedral (*a*) GeTe, $GeSe_{0.2}Te_{0.8}$ and $GeSe_{0.5}Te_{0.5}$, (*b*) Ge_4Se_3Te and (*d*) GeSe. The *c*/*a* ratios of the rhombohedral and hexagonal compounds are shown in (*c*).

The temperature dependences of the *c*/*a* ratios for the rhombohedral and hexagonal phases are shown in Fig. 2(*c*). At 300 K, they compare well with the values reported in the literature (Wiedemeier & Siemers, 1984; Küpers *et al.*, 2017; Bauer Pereira *et al.*, 2013). For the rhombohedral compounds, the *c*/*a* ratios decrease at higher temperature and increase with increasing Se content. The ideal *c*/*a* ratio derived from the transformation of a face-centred cubic cell to the *R*-centred cell (hexagonal setting) is 2.4495. Consequently, the stronger the deviation from this ratio, the more distorted the structure with respect to the cubic unit cell parameter corresponding to a primitive rhombohedral cell are shown in Fig. S3). For the rhombohedral structures, both the incorporation of Se and a decrease in the temperature lead to a larger deviation from the ideal *c*/*a* ratio [Fig. 2(*c*)]. At higher temperatures, the *c*/*a* ratio gets closer to the ideal value, which is finally reached at the phase transition to the f.c.c. phase (Wiedemeier & Siemers, 1984).

For the hexagonal Ge_4Se_3Te, a different temperature dependence of the lattice parameter is observed, as the *c*/*a* ratio increases with elevated temperatures [Fig. 2(*b*)]. One of the possible explanations for the different behaviour of the hexagonal compound might be the additional Ge···Ge bonding interactions and the presence of long-range Te···Te van der Waals contacts in the crystal structure of Ge_4Se_3Te, which are not present in GeTe.

A positive thermal expansion for all lattice parameters is observed in GeSe-I [Fig. 2(*d*)]. The *a* lattice parameter changes only slightly in the whole temperature range 25–300 K (about 0.1%). The influence of the temperature on the *b* and *c* lattice parameters of GeSe is nearly identical down to about 150 K. Below 150 K, they show a significantly different temperature dependence. This corresponds to the temperature below which new Raman modes were observed earlier (Fukunaga *et al.*, 1981). As there is no evidence of new peaks and/or changed intensity ratios in the powder data, we have no clear evidence for a structural phase transition. Hence, we cannot confirm the low-temperature phase transition proposed earlier (Fukunaga *et al.*, 1981).

3.2. High-pressure behaviour

A summary of the results from the high-pressure experiments on all compounds is shown in Fig. 3. GeTe, $GeSe_{0.2}Te_{0.8}$ and $GeSe_{0.5}Te_{0.5}$ undergo a phase transition from the GeTe-I to the f.c.c. GeTe-II type structure. The experimentally determined transition pressure increases with elevated Se-content: GeTe at 4.2 GPa → $GeSe_{0.2}Te_{0.8}$ at 5.8 GPa → $GeSe_{0.5}Te_{0.5}$ at 7.7 GPa. For GeTe and $GeSe_{0.2}Te_{0.8}$, the GeTe-II type is stable up to pressures above 20 GPa. For $GeSe_{0.5}Te_{0.5}$, it is only stable up to about 15 GPa (Table 3).

This indicates that the incorporation of Se into the structure reduces the stability field of the GeTe-II phases.

In order to directly compare the lattice parameters of the GeTe-I and GeTe-II type phases, their crystal structures have been transformed to the primitive rhombohedral unit cell [Figs. 4(*a*)–4(*c*)]. This is straightforward as the GeTe-I structure can be regarded as a distorted variant of a f.c.c. structure composed of Peierls-distorted octahedra. One can clearly see that the GeTe-I to GeTe-II transition is accompanied by a pronounced discontinuous change in the lattice parameters that indicates the first-order characteristics of the phase transition. As we have no evidence that the conditions during our high-pressure experiments were non-hydrostatic, our data imply that the discontinuities in lattice parameters observed in earlier studies (Leger & Redon, 1990; Serebryanaya *et al.*, 1995) are not necessarily a consequence of the non-hydrostatic conditions.

Using the unit-cell volume, a direct comparison of the influence of temperature, pressure and compositional parameter x is possible. Fig. 5 shows such a comparison for the c/a ratio of the compounds with rhombohedral structures. The increase of Se in the structure leads to a reduction of the unit cell volume and an increase in the deviation from the idealized c/a ratio corresponding to the cubic unit cell. Decreasing the unit cell volume by hydrostatic pressure has the opposite effect on the c/a ratio up to the transition pressure where the cubic GeTe-II phase is reached. The effect of temperature on unit-cell volume is comparatively small, yet an increase of the temperature leads to an approximation of the c/a ratio towards the ideal values corresponding to the cubic unit cell, which for GeTe, results in the observed phase transition to the GeTe-II structure at high temperatures at a critical volume of approximately 163.5 Å^3 (Wiedemeier & Siemers, 1984).

For all three compounds ($GeSe_xTe_{1-x}$ with x = 0, 0.2, 0.5), the GeTe-II phase co-exists with the newly determined orthorhombic GeTe-III phase at higher pressures, again hinting at a first-order phase transition. For $GeSe_{0.5}Te_{0.5}$, the two phases even co-exist over the whole stability field of the GeTe-II structure type. Using the lattice parameter of the GeTe-III phase as a starting point it was possible to index and subsequently refine the powder diffraction patterns of $GeSe_{0.2}Te_{0.8}$ and $GeSe_{0.5}Te_{0.5}$. Hence, the high-pressure polymorphs of these two compounds are most likely isotypical to the orthorhombic GeTe-III structure. For all three compounds, the orthorhombic phase is stable up to the highest pressures reached in the experiment.

Figs. 4(*d*)–4(*f*) shows the normalized lattice parameters of the GeTe-III phases. The pressure effect on the b and c lattice parameters is similar, while the pressure-induced changes of the a lattice parameter are largest with increasing Se content. This is expected, given that the layers of six membered rings are arranged perpendicular to the a axis in GeTe-III and the compression of the layers along [100] is hindered by Te···Te interactions. The Se—Se distances are shorter than the corresponding Te—Te distances, so with increasing Se content the layers are more compressible.

For the hexagonal Ge_4Se_3Te, no phase transition is observed up to 25 GPa [Fig. 3(*d*)]. The c direction is more influenced by the pressure than the a lattice parameter (see Fig. S4 of the supporting information). A comparison of the normalized lattice parameter of Ge_4Se_3Te to the ones of the GeTe-I phase of GeTe, $GeSe_{0.2}Te_{0.8}$ and $GeSe_{0.5}Te_{0.5}$ shows that the pressure-dependence of a is comparable for all compounds. In contrast to this, the pressure effect on c is more pronounced with elevated Se content. This trend also holds for hexagonal Ge_4Se_3Te. The crystal structure of the hexagonal phase consists of Te/Se–Ge–Ge–Te/Se layers, which are stacked on each other via van der Waals gaps along the [001] direction (Fig. 1). Within the ab plane, the bonding nature is dominated by heteroatomic Se/Te–Ge bonding, similar to the rhombo-

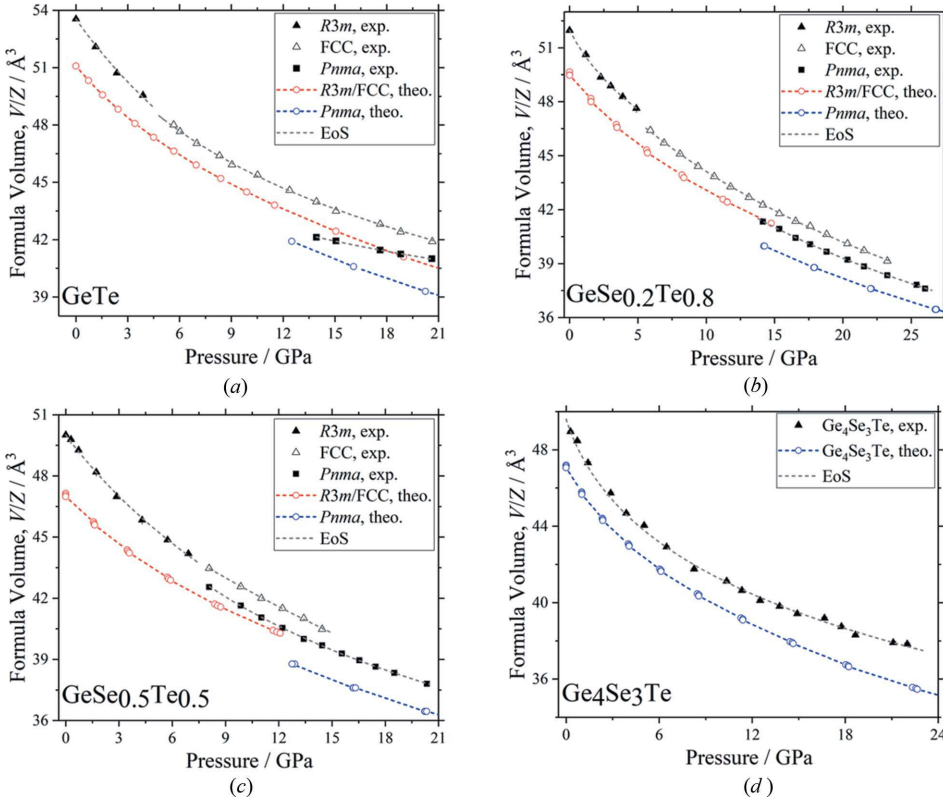

Figure 3
Pressure-induced phase transitions and equations-of-state of (*a*) GeTe, (*b*) $GeSe_{0.2}Te_{0.8}$, (*c*) $GeSe_{0.5}Te_{0.5}$ and (*d*) Ge_4Se_3Te. Equations-of-state as determined from first-principles calculations are shown for comparison.

Table 3
Bulk moduli, B_0 [first derivative of the bulk moduli fixed to $B' = 4$, exception Ge_4Se_3Te: $B' = 13$ (4) obtained from fit], formula unit volumes, V_i/Z, and transition pressure, p_{tr}, of GeTe, $GeSe_{0.2}Te_{0.8}$, $GeSe_{0.5}Te_{0.5}$ and Ge_4Se_3Te from experiment and theory.

For the rhombohedral GeTe-I structures, the values are given for ambient pressure (theory: 0 GPa); for the high-pressure phases GeTe-II and GeTe-III, the values at the transition pressure are listed. The modulus B_0 of hexagonal Ge_4Se_3Te was predicted for a pressure of 23 GPa which corresponds to the largest experimental pressure point.

	GeTe-I		GeTe-II			GeTe-III			
Compound	B_0 (GPa)	V_0/Z (Å^3)	p_{tr} (GPa)	B_{tr} (GPa)	V_{tr}/Z (Å^3)	p_{tr} (GPa)	B_{tr} (GPa)	V_{tr}/Z (Å^3)	
GeTe	35 (3)	53.55 (5)	4.2	68 (5)	48.51 (4)	13.9	205 (17)	42.14 (8)	Exp.
	54.5	51.089		118.9	40.19	13	106.1	41.66	DFT
$Ge_{0.2}Te_{0.8}$	45 (6)	51.8 (1)	5.8	74 (2)	46.4 (1)	13.2	104 (3)	41.4 (1)	Exp.
	49.9	49.687		109.2	39.73	11.4	97.4	41.10	DFT
$GeSe_{0.5}Te_{0.5}$	43 (4)	50.01 (1)	7.7	85 (4)	43.47 (5)	8.1	73 (3)	42.6 (1)	Exp.
	50.3	47.207		110.3	38.01	11.8	99.8	39.13	DFT
Hexagonal phase									
Ge_4Se_3Te	20 (4)	49.6 (5)							Exp.
	34.3	47.051							DFT

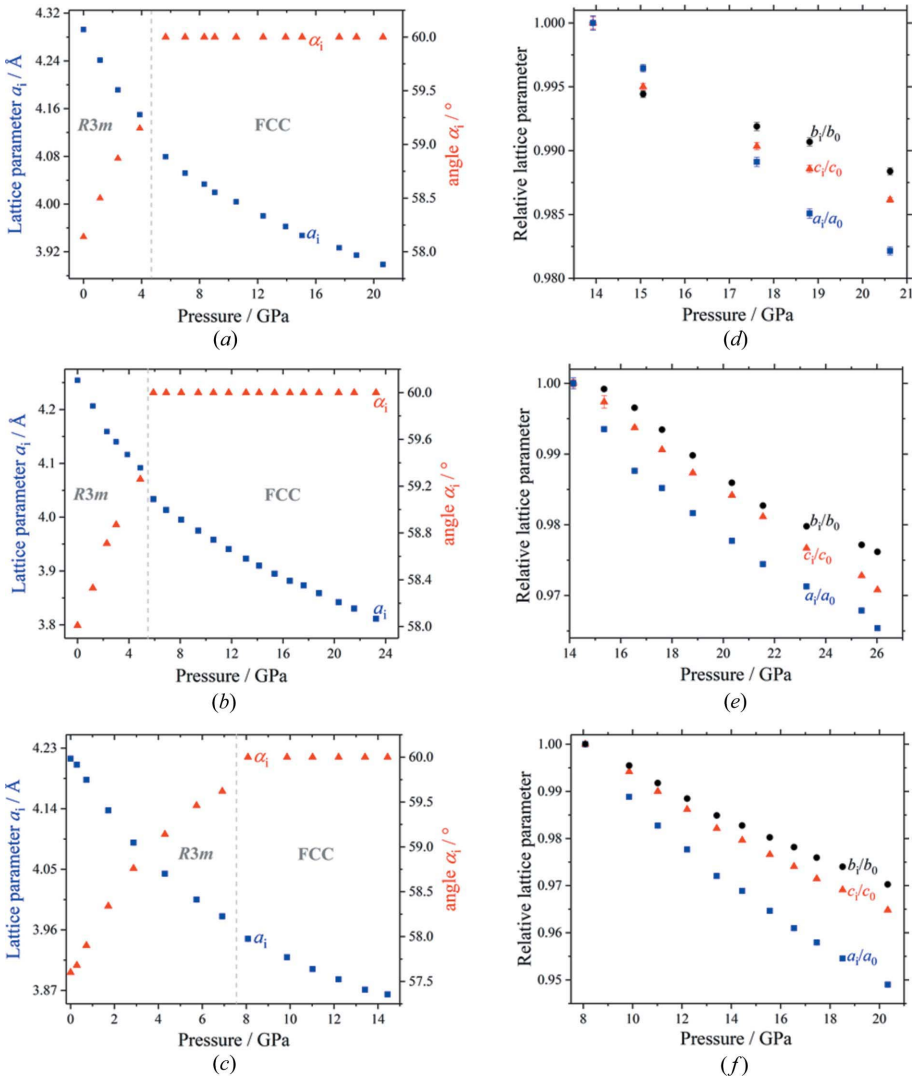

Figure 4
Primitive lattice parameter of the *R*3*m* and f.c.c. phase, respectively, of (*a*) GeTe, (*b*) $GeSe_{0.2}Te_{0.8}$ and (*c*) $GeSe_{0.5}Te_{0.5}$. In (*d*)–(*f*) the normalized lattice parameter of the GeTe-III polymorph of GeTe, $GeSe_{0.2}Te_{0.8}$ and $GeSe_{0.5}Te_{0.5}$ are depicted.

hedral phase, explaining the similar compressibility of *a*. However, the hexagonal phase shows homoatomic Ge—Ge bonding and Te/Se–Te/Se van der Waals interactions between the layers, which seem to increase the compressibility of the hexagonal phase along [001] when compared with the rhombohedral phase.

3.3. Bulk moduli

The *p*–*V* data for the rhombohedral GeTe-I phases and the hexagonal $GeSe_{0.75}Te_{0.25}$ were fitted with a third order Birch–Murnaghan equation-of-state using the program *EoSfit* (Gonzalez-Platas *et al.*, 2016). The bulk moduli (B_{tr}) and unit-cell volumes (V_{tr}) for the GeTe-II and GeTe-III phases at the observed transitions pressures (p_{tr}) were obtained using a Murnaghan equation-of-state (Menoni *et al.*, 1986). Fig. 3 shows the corresponding fits.

Table 3 compares bulk moduli obtained from our experiment and from first-principles calculations. The bulk modulus for GeTe-I obtained from the calculations is significantly overestimated. It agrees, however, fairly well with the value determined by Onodera *et al.* (1997). The experimental data suggest that the bulk modulus is initially increased when Se is incorporated into the GeTe-I structure. Further increase of the Se content has little influence on the bulk modulus. On the other hand, theory suggests an initial decrease of the bulk modulus when Te is replaced by Se. However, theory correctly reproduces the nearly identical bulk modulus for $GeSe_{0.2}Te_{0.8}$ and $GeSe_{0.5}Te_{0.5}$.

For the GeTe-II polymorphs, the experimental bulk moduli show an increase with increasing Se content, while the corresponding theoretical data suggest a slight decrease of the moduli. Altogether the influence of the Se content on the bulk modulus seems to be larger compared with the effect observed for the GeTe-I polymorphs. For the GeTe-III polymorphs, the experimentally determined moduli decrease significantly with increasing Se content, implying that the compressibility of the material is considerably

increased. This is a rather unexpected finding, as the Se/Te exchange leads to a reduction of the distance between neighbouring layers, and one would intuitively expect a reduction of the compressibility. The theoretical data for the GeTe-III phases do reflect this trend. However, the decrease of the bulk modulus with increasing Se content is far less pronounced than for the corresponding experimental data.

Despite the fact that the unit-cell volumes resulting from our chosen LDA *ansatz* are, in general, slightly underestimated when compared with the experimental values [Figs. 3(*a*)–3(*d*)], the significant discontinuities at the transition from the GeTe-II to the GeTe-III phases are nicely reproduced for the $GeSe_xTe_{1-x}$ (x = 0, 0.2, 0.5) compounds in the theoretical calculations.

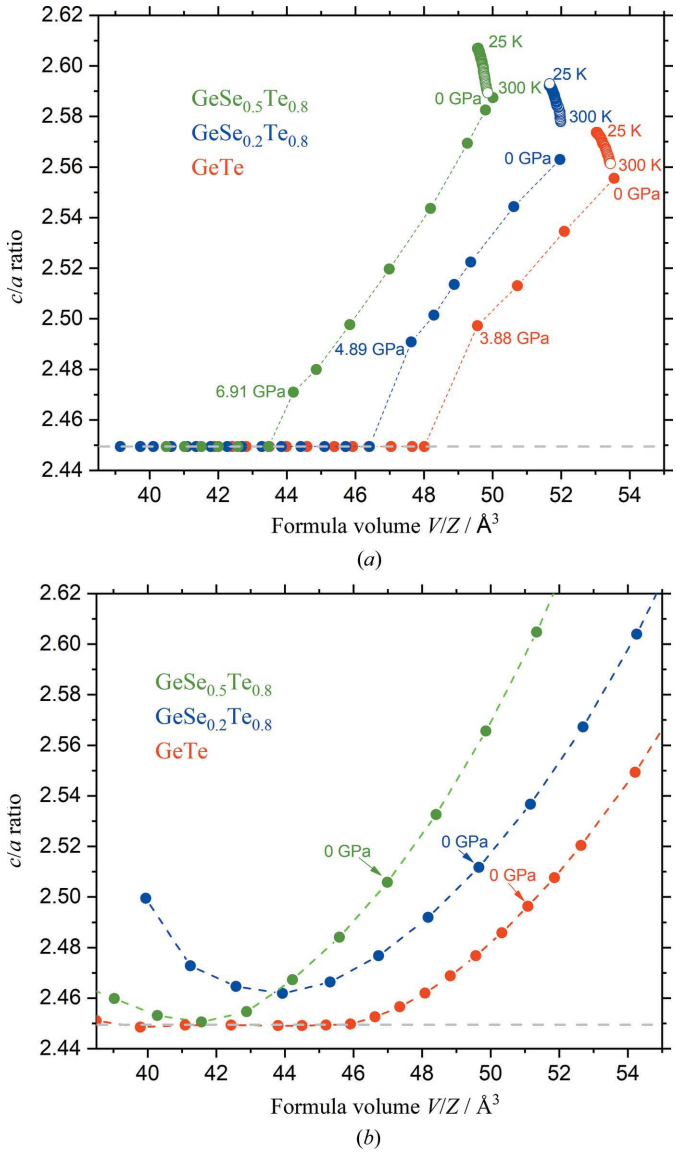

Figure 5
(*a*) Experimental and (*b*) predicted *c*/*a* ratio for the rhombohedral compounds as a function of the formula volume. Temperature-dependent data at ambient pressure are shown as open symbols, pressure-dependent experimental and theoretical data at ambient temperature as closed ones.

For hexagonal Ge_4Se_3Te, the experiments yield a bulk modulus of B_0 = 20.0 (5) GPa, which is in poor agreement with the theoretically determined value of 34.3 GPa. However, the experimentally determined unit-cell volume is in excellent agreement with earlier results (Küpers *et al.*, 2017).

In order to understand the high-pressure behaviour of the $GeSe_xTe_{1-x}$ system, we have calculated the enthalpies as functions of pressure for GeTe, $GeSe_{0.2}Te_{0.8}$, $GeSe_{0.5}Te_{0.5}$ and $GeSe_{0.75}Te_{0.25}$ in the GeTe-I/GeTe-II, GeSe-I/GeSe-II (*Pnma*/*Cmcm*) structures, the hexagonal ($P6_3mc$) and the orthorhombic GeTe-III (*Pnma*) structures based on first-principles calculations (Fig. 6). In the figure, the enthalpy differences of the high-pressure phases relate to the enthalpy of the GeTe-I/GeTe-II structure which was set to zero. We found, in agreement with the experimental results, that the GeTe-I/GeTe-II structures are energetically favourable at ambient pressure for isostructural GeTe, $GeSe_{0.2}Te_{0.8}$ and $GeSe_{0.5}Te_{0.5}$. At higher pressures of about 12–13 GPa, the enthalpy of the GeTe-III structure becomes smaller than that of the GeTe-I/GeTe-II phase, indicating that the GeTe-III structure is energetically favourable, in agreement with our experimental observations. While for GeTe and $GeSe_{0.2}Te_{0.8}$ the calculations nicely reproduce the experimental transition pressures, the transition pressure is slightly overestimated for $GeSe_{0.5}Te_{0.5}$ (see Table 3).

The first-principles calculations for hexagonal Ge_4Se_3Te suggest that at ambient pressure, the GeTe-I/GeTe-II structure is energetically more favourable than the $P6_3mc$ structure by about 1 kJ mol^{-1}. This clearly indicates that the $P6_3mc \rightarrow$ GeTe-I/GeTe-II transition is sterically hindered. The $P6_3mc$ structure can be considered as a GeTe-I structure in which each second layer is rotated by 180° along the [010] direction, and the activation energy for this rotation is likely much larger than 1 kJ mol^{-1}. Furthermore, the DFT calculations show that the GeTe-III type structure is energetically favourable over the GeTe-I/GeTe-II phase above about 5 GPa. Again, this is in discrepancy to the experimental results, but can be ascribed to the steric hindrance of the hexagonal phase.

3.4. Comparison of the different structure types and bonding analysis

Fig. 1 shows a comparison of the different structures in the $GeSe_xTe_{1-x}$ system. All of these phases, except for the f.c.c. GeTe-II phase, are composed of layers of six-membered Ge-Te/Se rings as marked in the figure. GeTe-III is isotypic to β-GeSe, which was synthesized from GeSe-I at high temperature and pressure (von Rohr *et al.*, 2017). In GeTe-I, the six-membered rings are arranged in the *chair* conformation, while in the structures of GeTe-III and β-GeSe, the six-membered Ge—Te rings are arranged in the *boat* conformation. We do not include the two former models proposed for the GeTe-III phase (Onodera *et al.*, 1997; Serebryanaya *et al.*, 1995) in the comparison, as both of them do not index our diffraction patterns. In addition, the model proposed by Onodera *et al.* (1997) leads to unreasonably short Ge—Te distances.

In the lower part of Fig. 1, the coordination of Ge in the different phases is compared. In the structure of GeTe-II, the Ge atom is coordinated by Te in the form of an undistorted octahedron, while in GeTe-I the octahedron shows a Peierls distortion, leading to a [3 + 3] coordination with three shorter covalent Ge—Te bonds and three longer Ge···Te interactions (Bauer Pereira *et al.*, 2013). In Ge_4Se_3Te, Ge also shows a [3 + 3] coordination, which is formed by three covalent Ge—Te/Se bonds and three Ge···Ge interactions (Bauer Pereira *et al.*, 2013). In GeSe-I, GeTe-III and β-GeSe, the Ge atoms are surrounded by three short Ge—Te (Se) bonds, three long Ge—Te (Se) bonds and two Ge···Ge interactions. For GeTe-III at 18.8 GPa, an additional even longer bond to Te (shown in grey) appears to be important (see discussion below).

The bonding analysis on GeTe-III at 0 and 15 GPa was carried out with the crystal orbital Hamilton population (COHP) method. The integrated COHP (ICOHP) was utilized as a measure of the bond strength between two atoms. Usually, strong bonding interactions are characterized by ICOHP values of the order of one electronvolt or more, just as covalent bonds are of the order of hundreds of kJ mol^{-1}. It is useful to then compare the relative strength of the bonds from the course of the ICOHP values. Fig. 7 shows the COHPs for selected bonds.

Table 4
Theoretical bond lengths of the GeTe-III structure at 0 and 15 GPa compared with the experimentally determined values at 18.8 GPa together with the ICOHP values.

Bond	Type	$d_{th,0\ GPa}$ (Å)	$ICOHP_{0\ GPa}$ (eV)	$d_{th,15\ GPa}$ (Å)	$ICOHP_{0\ GPa}$ (eV)	$d_{exp,18.8\ GPa}$ (Å)	
(a)	Ge—Te	2.756	−3.324	2.689	−3.426	2.684 (9)	
(b)	Ge—Te	2.811	−2.860	2.749	−2.804	2.746 (7)	2×
(c)	Ge—Te	3.178	−1.062	2.874	−1.904	2.888 (7)	2×
(d)	Ge—Ge	3.457	−0.437	2.959	−1.259	2.971 (7)	2×
(e)	Ge—Te	3.421	−0.451	3.180	−0.581	3.208 (10)	
(f)	Ge—Te	3.971	−0.053	3.384	−0.258	3.396 (10)	

The GeTe-III structure exhibits a large variety of bonds, including next-neighbour Ge···Ge interactions. The six nearest-neighbour interactions, of which three are degenerate, were included, leading to nine nearest interactions (compare Fig. 1). Table 4 shows the bond lengths of the optimized structures at 0 and 15 GPa compared to the experimentally determined ones at 18.8 GPa.

The two shortest Ge—Te bonds (a) and (b) shrink only slightly under pressure and do not significantly differ in terms of their ICOHP values at 0 and 15 GPa. However, the COHP of bond (a) shows antibonding interactions below the Fermi level which disappear at 15 GPa where, up to the Fermi level, there are only bonding interactions (Fig. 7). This reflects the stabilization of the structure under pressure.

The length of the shortest Ge—Ge bond (d) decreases by approximately 0.5 Å, from 3.46 to 2.96 Å. Compared with the Ge—Te bond of similar length at ambient pressure (e), this decrease is significantly more important. The ICOHP value of the Ge—Ge bond is three times as large at 15 GPa (−1.26 eV) compared with that at ambient pressure (−0.44 eV), while the ICOHP value of the comparable Ge—Te bond increases only slightly at higher pressure.

The longest given Ge—Te distance (f) (indicated also in Fig. 1) decreases (theoretically) from 3.97 to 3.38 Å, and its ICOHP value also increases significantly from −0.05 eV to −0.26 eV (a more negative value indicates greater stability because the energy lowers). Compared with the contributions from the other bonds, at ambient pressure it can be neglected as a bonding interaction, however, at 15 GPa, there is a significant interaction. This might indicate that at pressures higher than the ones reached in this study, the coordination number around Te would increase even further.

Our results show that the stabilization of the GeTe-III structure under pressure is related to the strength-

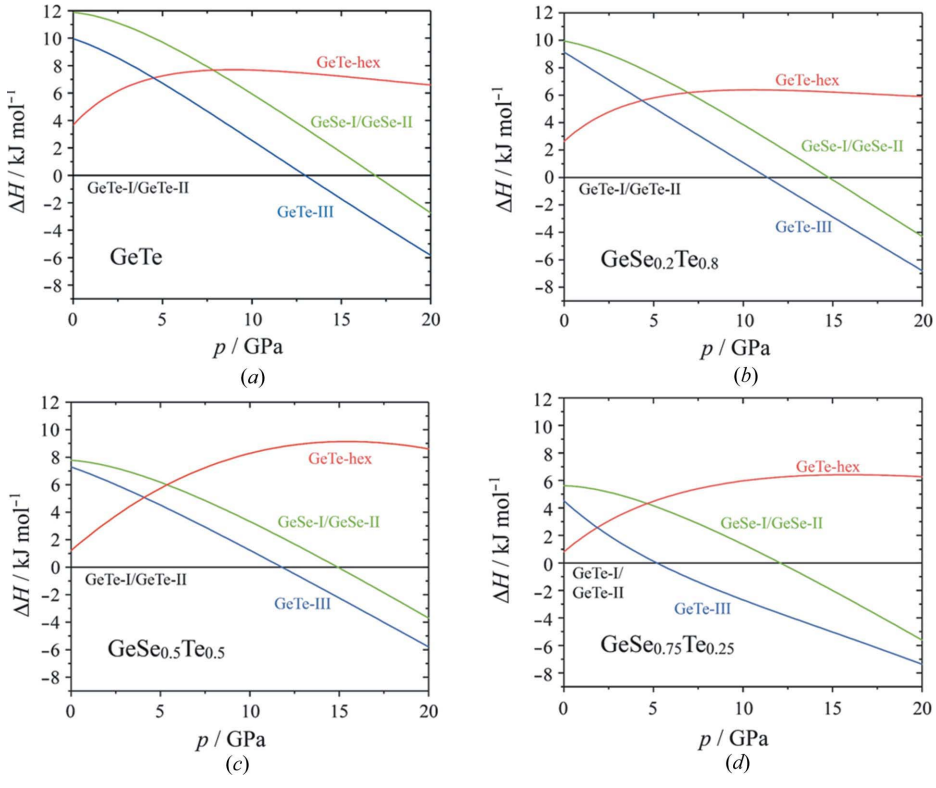

Figure 6
Predicted enthalpy differences between the fictive HP phases of (*a*) GeTe, (*b*) $GeSe_{0.2}Te_{0.8}$, (*c*) $GeSe_{0.5}Te_{0.5}$ and (*d*) Ge_4Se_3Te. Enthalpy values of the GeTe-I/GeTe-II structures were set to zero.

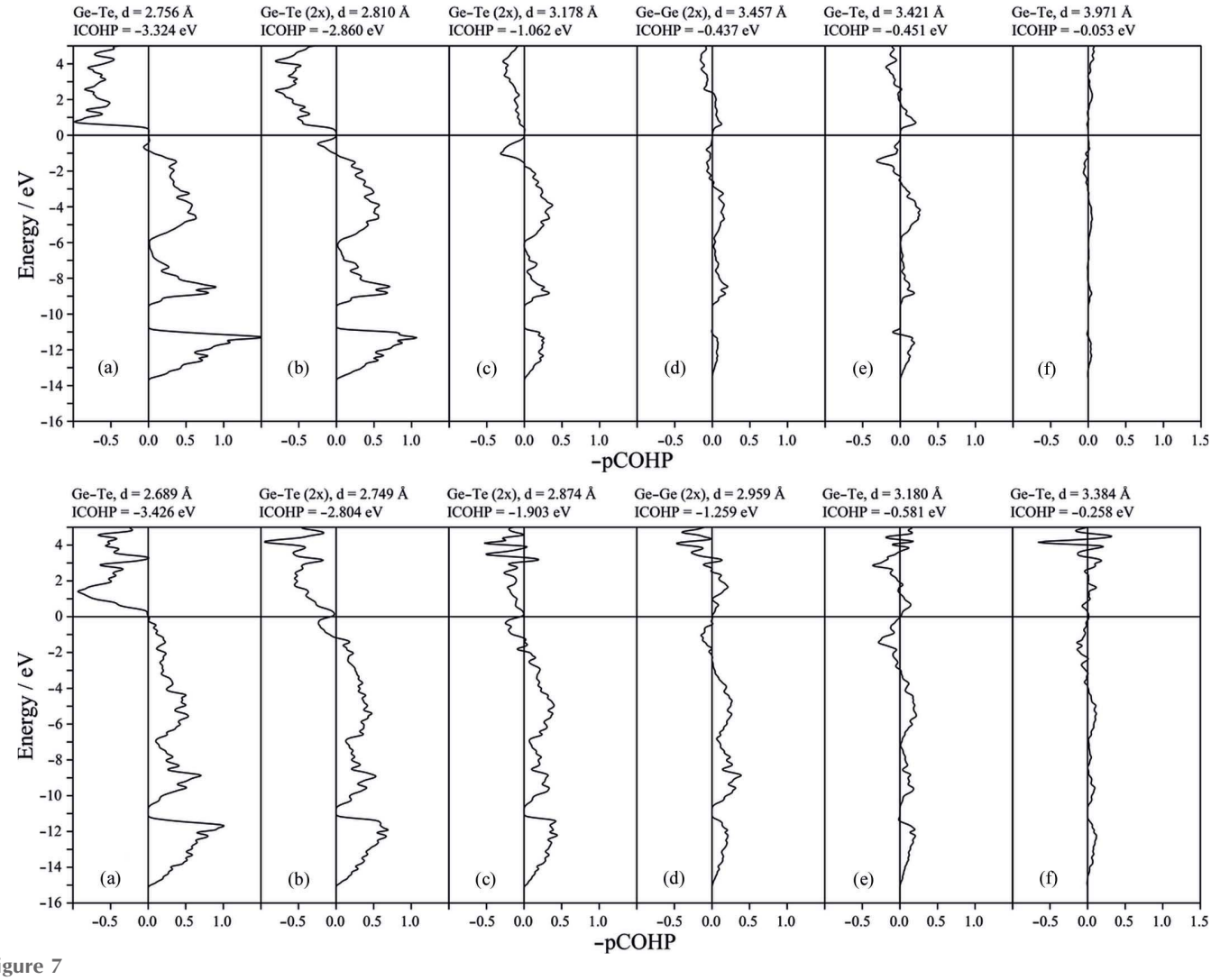

Figure 7
COHP plots of selected bonds within the GeTe-III structure at 0 GPa (top) and 15 GPa (bottom). Positive COHP values indicate bonding interactions whereas negative COHP represent antibonding states.

ening of two Ge—Te bonds (c) and (f) and one Ge—Ge bond (d) together with the absence of antibonding interactions up to the Fermi level within the shortest Ge—Te bond (a).

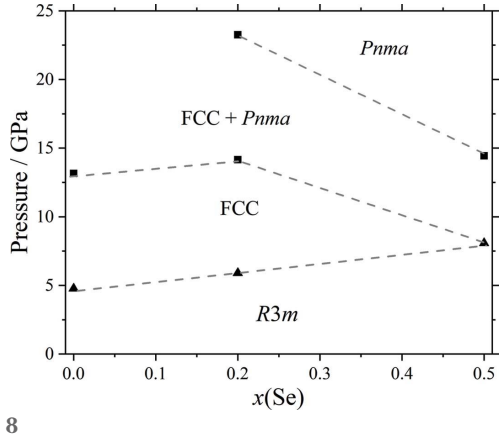

Figure 8
Tentative high-pressure phase diagram of the $GeSe_xTe_{1-x}$ solid solution for x(Se) between 0 and 0.5.

4. Conclusions

Temperature-dependent experiments show that the compounds in the system $GeSe_{1-x}Te_x$ with a GeTe-type structure exhibit a positive thermal expansion along the [001] direction while hexagonal Ge_4Se_3Te exhibits negative thermal expansion along this direction. This can be explained by the presence of additional Ge···Ge interactions in the hexagonal compound. The crystal structure of pressure-induced GeTe-III (*Pnma*), isostructural to β-GeSe, has been determined, and existing contradictions in the literature with respect to its structure have been resolved. Additional Ge···Ge interactions in this structure are formed due to the change of the six-membered Ge—Te rings from a *chair* to a *boat* conformation. Fig. 8 shows a sketch of the high-pressure phase diagram. All the compounds with the GeTe structure type follow the high-pressure transition pathway: $R3m \rightarrow$ f.c.c. $\rightarrow Pnma$. The pressure of the $R3m \rightarrow$ f.c.c. transition increases with increasing Se content. In contrast to this, the transition pressure to the GeTe-III phase is lowered upon increasing Se content. The

high-pressure polymorphs GeTe-II and GeTe-III co-exist over a wide pressure range. Bonding analysis carried out with the COHP method shows that the stabilization of the GeTe-III structure under pressure is due to the strengthening of two of the longer Ge—Te bonds and of the Ge···Ge interactions. The structure of Ge_4Se_3Te is stable up to at least 25 GPa.

Acknowledgements

Part of this research was performed on beamline P02.2 at Petra III. We would like to thank H.-P. Liermann for support during our measurements.

Funding information

We thank the Deutsche Forschungsgemeinschaft for financial support (within SFB 917 'Nanoswitches') and the Jülich–Aachen Research Alliance as well as the IT Centre at RWTH Aachen University for providing CPU time (JARA-HPC project jara0033). We acknowledge DESY (Hamburg, Germany), a member of the Helmholtz Association, HGF, for the provision of experimental facilities.

References

Alptekin, S. & Durandurdu, M. (2010). *Solid State Commun.* **150**, 870–874.

Bansal, D., Hong, J., Li, C. W., May, A. F., Porter, W., Hu, M. Y., Abernathy, D. L. & Delaire, O. (2016). *Phys. Rev. B*, **94**, 054307.

Bauer Pereira, P., Sergueev, I., Gorsse, S., Dadda, J., Müller, E. & Hermann, R. P. (2013). *Phys. Status Solidi B*, **250**, 1300–1307.

Blöchl, P. E. (1994). *Phys. Rev. B*, **50**, 17953–17979.

Burla, M. C., Caliandro, R., Carrozzini, B., Cascarano, G. L., Cuocci, C., Giacovazzo, C., Mallamo, M., Mazzone, A. & Polidori, G. (2015). *J. Appl. Cryst.* **48**, 306–309.

Cardona, M. & Greenaway, D. L. (1964). *Phys. Rev.* **133**, A1685–A1697.

Ceperley, D. M. & Alder, B. J. (1980). *Phys. Rev. Lett.* **45**, 566–569.

Deringer, V. L., Stoffel, R. P., Wuttig, M. & Dronskowski, R. (2015). *Chem. Sci.* **6**, 5255–5262.

Deringer, V. L., Tchougréeff, A. L. & Dronskowski, R. (2011). *J. Phys. Chem. A*, **115**, 5461–5466.

Dronskowski, R. & Bloechl, P. E. (1993). *J. Phys. Chem.* **97**, 8617–8624.

Fukunaga, T., Sugai, S., Kinosada, T. & Murase, M. (1981). *Solid State Commun.* **38**, 1049–1052.

Gonzalez-Platas, J., Alvaro, M., Nestola, F. & Angel, R. (2016). *J. Appl. Cryst.* **49**, 1377–1382.

Hein, R. A., Gibson, J. W., Mazelsky, R., Miller, R. C. & Hulm, J. K. (1964). *Phys. Rev. Lett.* **12**, 320–322.

Kantor, I., Prakapenka, V., Kantor, A., Dera, P., Kurnosov, A., Sinogeikin, S., Dubrovinskaia, N. & Dubrovinsky, L. (2012). *Rev. Sci. Instrum.* **83**, 125102.

Karbanov, S. G., Zlomanov, V. P. & Novoselova, A. V. (1968). *Dokl. Chem.* **182**, 862–863.

Kresse, G. & Furthmüller, J. (1996). *Phys. Rev. B*, **54**, 11169–11186.

Kresse, G. & Joubert, D. (1999). *Phys. Rev. B*, **59**, 1758–1775.

Küpers, M., Konze, P. M., Maintz, S., Steinberg, S., Mio, S. M., Cojocaru-Mirédin, O., Zhu, M., Müller, M., Luysberg, M., Mayer, J., Wuttig, M. & Dronskowski, R. (2017). *Angew. Chem. Int. Ed.* **56**, 10204–10208.

Lee, S., Esfarjani, K., Luo, T., Zhou, J., Tian, Z. & Chen, G. (2014). *Nat. Commun.*, **5**, 3525.

Leger, J. M. & Redon, A. M. (1990). *J. Phys. Condens. Matter*, **2**, 5655–5662.

Lencer, D., Salinga, M., Grabowski, B., Hickel, T., Neugebauer, J. & Wuttig, M. (2008). *Nat. Mater.* **7**, 972–977.

Levin, E. M., Besser, M. F. & Hanus, R. (2013). *J. Appl. Phys.* **114**, 083713.

Lewis, J. E. (1974). *Phys. Lett. A*, **47**, 404–406.

Li, J., Chen, Z., Sun, Y., Yang, J. & Pei, Y. (2017). *NPG Asia Materials*. **9**, e353.

Maintz, S., Deringer, V. L., Tchougréeff, A. L. & Dronskowski, R. (2013). *J. Comput. Chem.* **34**, 2557–2567.

Maintz, S., Deringer, V. L., Tchougréeff, A. L. & Dronskowski, R. (2016). *J. Comput. Chem.* **37**, 1030–1035.

Mao, H. K., Xu, J. & Bell, P. M. (1986). *J. Geophys. Res.* **91**, 4673–4676.

Menoni, C. S., Hu, J. Z. & Spain, I. L. (1986). *Phys. Rev. B*, **34**, 362–368.

Monkhorst, H. J. & Pack, J. D. (1976). *Phys. Rev. B*, **13**, 5188–5192.

Okoye, C. M. I. (2002). *J. Phys. Condens. Matter*, **14**, 8625–8637.

Onodera, A., Sakamoto, I., Fujii, Y., Mori, N. & Sugai, S. (1997). *Phys. Rev. B*, **56**, 7935–7941.

Pecharsky, V. K. & Zavalij, P. Y. (2003). *Fundamentals of Powder Diffraction and Structural Characterization of Materials*, 1st ed. New York: Springer Science & Business Media.

Perdew, J. P. & Zunger, A. (1981). *Phys. Rev. B*, **23**, 5048–5079.

Perumal, S., Roychowdhury, S. & Biswas, K. (2016). *J. Mater. Chem. C.* **4**, 7520–7536.

Petricek, V., Dusek, M. & Palatinus, L. (2014). *Z. Kristallogr. Cryst. Mater.* **229**, 345–352.

Prescher, C. & Prakapenka, V. B. (2015). *High Pressure Res.* **35**, 223–230.

Rigaku Oxford Diffraction (2015). *CrysAlis PRO*. Rigaku Oxford Diffraction Ltd, Yarnton, Oxfordshire, UK.

Rohr, F. O. von, Ji, H., Cevallos, F. A., Gao, T., Ong, N. P. & Cava, R. J. (2017). *J. Am. Chem. Soc.* **139**, 2771–2777.

Serebryanaya, N. R., Blank, V. D. & Ivdenko, V. A. (1995). *Phys. Lett. A*, **197**, 63–66.

Shportko, K., Kremers, S., Woda, M., Lencer, D., Robertson, J. & Wuttig, M. (2008). *Nat. Mater.* **7**, 653–658.

Stoffel, R. P., Deringer, V. L., Simon, R. E., Hermann, R. P. & Dronskowski, R. (2015). *J. Phys. Condens. Matter*, **27**, 085402.

Taube, A., Łapińska, A., Judek, J., Wochtman, N. & Zdrojek, M. (2016). *J. Phys. D Appl. Phys.* **49**, 315301.

Wiedemeier, H. & Siemers, P. A. (1984). *High Temp. Sci.* **17**, 395–408.

Wiedemeier, H. & von Schnering, H. G. (1978). *Z. Kristallogr.* **148**, 295–303.

Xu, M., Jakobs, S., Mazzarello, R., Cho, J.-Y., Yang, Z., Hollermann, H., Shang, D., Miao, X., Yu, Z., Wang, L. & Wuttig, M. (2017). *J. Phys. Chem. C*, **121**, 25447–25454.

Yang, L., Li, J. Q., Chen, R., Li, Y., Liu, F. S. & Ao, W. Q. (2016). *J. Electron. Mater.* **45**, 5533–5539.

Zhang, J., Zhu, H., Wu, X., Cui, H., Li, D., Jiang, J., Gao, C., Wang, Q. & Cui, Q. (2015). *Nanoscale*, **7**, 10807–10816.

Zurhelle, A. F., Deringer, V. L., Stoffel, R. P. & Dronskowski, R. (2016). *J. Phys. Condens. Matter*, **28**, 115401.